Advanced LIGO Seismic Isolation System Conceptual Design

J. Giaime, B. Lantz, C. Hardham, W. Hua,

R. Adhikari, D. Debra, G. Hammond, J. Hammond,

J. How, S. Richman, J.Rollins,G. Stapfer, R. Stebbins

January 20, 2001. `LIGO-E010016-00-D`

Contents

1 Introduction

The seismic isolation needed for Advanced LIGO requires a significant technological change from the system used in the initial LIGO detector. To take advantage of the improved thermal noise of a 30-40 kg test mass made of high-Q material and suspended with fused silica fibers, one must attenuate the ground motion by more than nine orders of magnitude at 10 Hz. Active isolation of ground motion to reduce the root-mean-squared ground displacement and the displacement noise in the gravitational wave band, coupled with multiple pendulum suspensions, address this requirement. The conceptual design for the active seismic isolation system is described in this document.

The design uses one stage external to the vacuum system and two stages inside the vacuum. These stages are mechanically connected with stiff springs, with typical passive resonances in the 2-4 Hz range. **Active isolation using feedback:** For the inner stages, we measure motion in all 6 degrees of freedom (DOF) for each stage, filter those signals, and feed them back to non-contacting force actuators between the stages, reducing the noise by a factor of the servo loop gain. **Active isolation using feed-forward:** For the outside stage, we reduce noise by measuring the floor motion, and feeding the negative of this signal forward, filtered by the modeled mechanical transmission, floor-to-stage, thus cancelling most of the transmitted noise. This cancellation, here largely confined to lower frequencies, is limited by our knowledge of the system's transmission properties.

1.1 Motion requirements and interface

Advanced LIGO's test mass suspension system is being developed by the GEO group at the University of Glasgow[6]. The interface between it and SEI as well as the performance requirements on SEI are set out in [2]. A well-defined interface has been chosen in order to allow independent testing of the two detector subsystems, and to facilitate their separate parallel development on different continents.

The BSC geometry requires SEI to support its payload from above, and so will feature a downward-facing matrix-drilled optics-table-like surface; The HAM geometry requires payload support from below, so will have an upward-facing optics table. This will require two different versions of our SEI design. A conceptual reference design has been chosen that limits the BSC/HAM differences to the interface and stage structures; the sensing, actuation, and control instrumentation that carries out the active isolation is identical in the two versions. In addition, the motion sensing and actuation is largely confined to "pods," which are field removable for service and replacement without disturbing the optics. These pods are also identical in the BSC and HAM designs. We expect that the performance and the implementation challenges of the two systems will be similar, so we will not generally differentiate between the two versions when describing the technology in this document.

1.2 Functional breakdown

The overall design consists of a hydraulic actuator outside the vacuum chamber and a two-stage active seismic isolation platform inside the chamber. Figure 1 shows the roles of the various parts of the SEI and SUS in LIGO-I and Advanced LIGO.

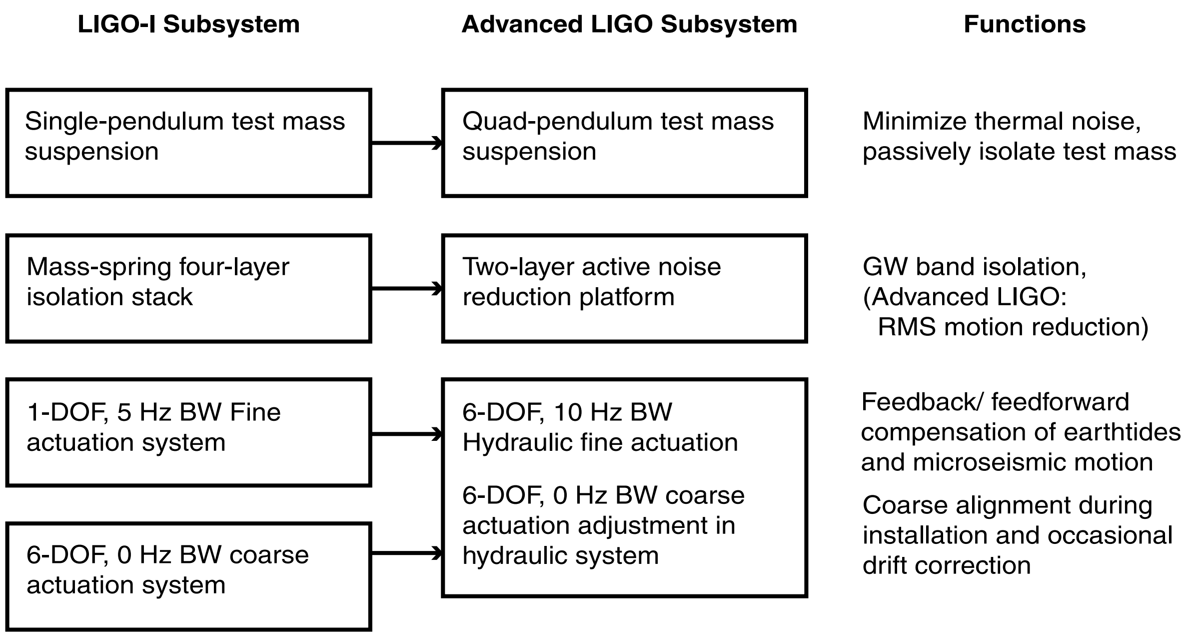

Figure 1: Seismic isolation functions in LIGO-I and Advanced LIGO, broken down by subsystem. Note that the present fine and coarse actuators are replaced by a hydraulic system in this design, and that an additional function, RMS motion reduction, is now required. The pendulum suspension, though not part of SEI, is shown because it contributes significant seismic isolation.

The present external fine actuators are used in LIGO-I to translate, only in the beam direction, the in-vacuum SEI systems by ± 90 μm with an actuation bandwidth of several hertz. LIGO-I also has coarse actuators that can move ± 5 mm. These systems will be replaced with a **quiet hydraulic actuator** that can move the in-vacuum SEI components by ± 1 mm with a bandwidth of 10 Hz in all six degrees of freedom. This should allow higher performance feed-forward correction of low-frequency ground noise and sufficient dynamic range for Earth tides and thermal or seasonal drifts. We expect approximately a factor of 10 reduction of the microseismic ($3 \times 10^{-2} - 3 \times 10^{-1}$ Hz) motion, from feedforward correction in this stage. There is also the possibility of using this stage in conjunction with a precision tilt sensor to servo the entire in-vacuum SEI to a global level.

The LIGO-I seismic isolation stack will be replaced with a **two-stage active seismic isolation platform.** As introduced above, vibration in each of the two cascaded stages is reduced by sensing its motion in 6 DOF's and applying forces in feedback loops to reduce the sensed motion. The outer stage derives its feedback signal by blending three real sensors for each DOF—a long-period broadband seismometer, a short-period geophone, and a relative position sensor. The inner stage lacks the long-period seismometer, so has less feedback gain at low frequencies, including the microseismic frequencies. However, the low noise floor of the outer stage seismometer allows feedforward correction to the inner stage, and we expect an additional factor of 10 reduction in that range. Performance is described in greater detail in section 3.

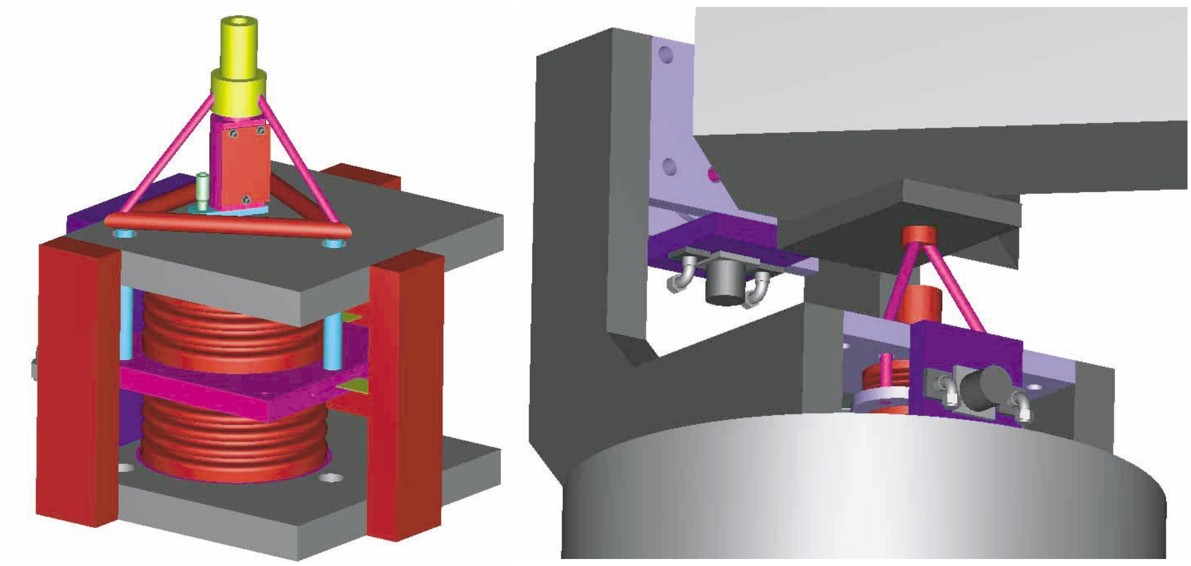

Figure 2: The Quiet Hydraulic Actuator. The gray blocks and red pillars form the reaction frame and are fixed in place. The two red bellows are pumped differentially to move the center purple actuation plate. The yellow bolt at the top attaches to the payload, and the actuation plate is attached to the payload by the rod assembly. An optical sensor (red and magenta) is placed between the yellow actuation point and the frame to allow low frequency servo stabilization. The figure at right shows two single-DOF actuators in place at the top of a SEI pier.

2 Design Description

2.1 Hydraulic external actuation

Conventional hydraulic actuators are found in many high force positioning applications. The conventional approach is not applicable here because of the high frequency fluid noise generated at all internal orifices. The field of quiet hydraulics is based on maintaining laminar flow throughout a system so as to eliminate high-frequency noise caused by turbulence. The conceptual design includes a quiet hydraulic external actuator to continuously control large displacements of the SEI payload via control reallocation from the more sensitive loops, and via feedforward based on signals from floor-mounted long-period seismometers.

The bandwidth and range described above can be achieved with a fluid working pressure of about 100 psi, one or more orders of magnitude less than conventional hydraulic designs. The pump power requirements remain modest by virtue of the relatively low upper unity gain point at 10 Hz. Since the velocities involved are extremely small (on the order 100 μm/s) with vertical actuation of a 2000 kg mass, the power requirements are quite small, approximately 2 W for the combined vertical actuators. Only a few tens of watts of pumping power are needed per chamber, and we plan to put the pump away from the LVEA/VEA slabs. The quiet hydraulic actuator (Figure 2) is mechanically similar to a standard hydraulic piston. However, in order to avoid the stiction and leakage associated with conventional pistons, bellows are used as actuation cavities. The system runs with a viscous working fluid, mineral oil, and is engineered to maintain laminar flow while ensuring the hydraulic

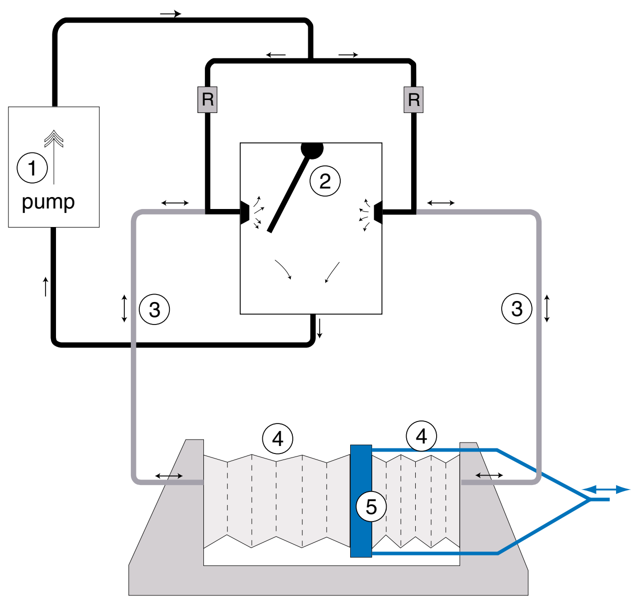

1. Viscous hydraulic fluid is pumped continuously into the control valve from 2 sides, and fluid is returned from a common point.

2. The control valve can move between the two inlets, creating a pressure differential on the different sides of the valve. The hydraulic resistance of the input lines (R) is balanced, so this system becomes the hydraulic equivalent of a Wheatstone bridge.

3. Tubing connects the two sides of the valve to the two sides of the differential bellows.

4. The differential bellows move when the pressure on the two sides is different.

5. The middle plate is attached in with flexures to both the base and the payload. The actuation point is constrained to apply force in one dimension, but is soft in all other degrees of freedom.

6. An optical displacement sensor is placed between the moving block and the frame for servo stabilization.

Figure 3: Flow diagram of a single quiet hydraulic actuator.

resonances are kept above 40 Hz. Figure 3 describes the continuous-laminar-flow differential-actuation scheme.

A displacement is commanded by closing a local servo loop on the hydraulic control valve based on a sensor that measures the 1-D displacement between the moving middle plate (between the bellows) and the frame. The local sensor will be chosen so that its noise won't compromise the overall system performance; an optical imaging sensor is a likely choice.

The displacement will be held against a hydraulic stiffness associated with a natural frequency of about 10 Hz. The hydraulic actuator we are developing will have an impedance that changes from being dominated by its support spring to being dominated by the viscous resistance at about 0.1 Hz. Thus, the velocity if accidently released at full stroke will be less that 1 mm/s. It will return to its rest position with a smooth exponential decay.

Coarse actuation: The continuous DC force of gravity will be off-loaded from the vertical actuators via short, very stiff, coil springs angled in "vee" pairs from the payload to frames on the SEI piers. The external SEI is required to facilitate periodic off-line alignment equivalent to $\pm$1mm at each actuator. This may be done as follows: The hydraulic system is used to move the payload to its new position. Then, while monitoring the hydraulic error signals, the spring tensions are manually adjusted until these error signals are very low. Finally, the hydraulic actuators are detached and recentered. The only abrupt forces that the system may see is the unbalanced hydraulic bellows stiffness. This process may be repeated to allow excursions larger than 1 mm.

2.2 Two-stage active isolation platform

Figures 4 and 5 show the BSC and HAM configurations of the cascaded two-stage active isolation platform. The stages are suspended through stiff blade springs and short pendulum links, giving natural frequencies in the 2 - 8 Hz range. This high suspension frequency means that the system's expansion sensitivity to temperature is about what you would expect from solid metal of the same linear dimension. The inner platform stage is built around a 1.5 m diameter optics table (BSC) or a larger rectangular table (HAM). For each suspended optic, the SUS is mounted on this flat table, and may be positioned and oriented as desired.

Local damping and noise-reduction control signals are generated for each DOF using a blended signal derived from short- and long-period seismometers and relative position sensors, which are described in section 2.2.1. The actuators are electromagnetic non-contacting forcers, which apply forces between adjacent stages, and are also described in 2.2.1.

The two-stage active seismic isolation platform resembles the pre-prototype built and tested at JILA over the past decade [7]. However, it has been refined and extended based on ideas and experimental work carried out at Stanford. The JILA development effort was directed towards a different goal (to detect GWs at 1 Hz), so our design has benefited from the JILA experience and 3-D modelling effort without the need for the ultra-high-performance seismometers that were part of JILA's development work (and impediments to robust operation). Instead, we will use commercial, off-the-shelf seismometers, greatly simplifying the scheme and reducing risk. The choice of stiffer suspension also promises better thermal drift performance. The JILA experience, plus Stanford work (see, for example, [8]) on optimal sensor blending, feedforward techniques, together with a new understanding of the benefits of stiff suspension, and large (1 mm) mechanical clearances, have led to our conceptual reference design. The less flexible JILA dynamic model has now been retired in favor of that described below (section 3) and in [4] and [3].

2.2.1 Sensors and actuators

We have identified a set of sensors and actuators, described below, that are appropriate for the Advanced LIGO isolation system. We are currently testing all but the capacitive displacement sensors in our two pre-prototype experiments, further described in [5]. Parts

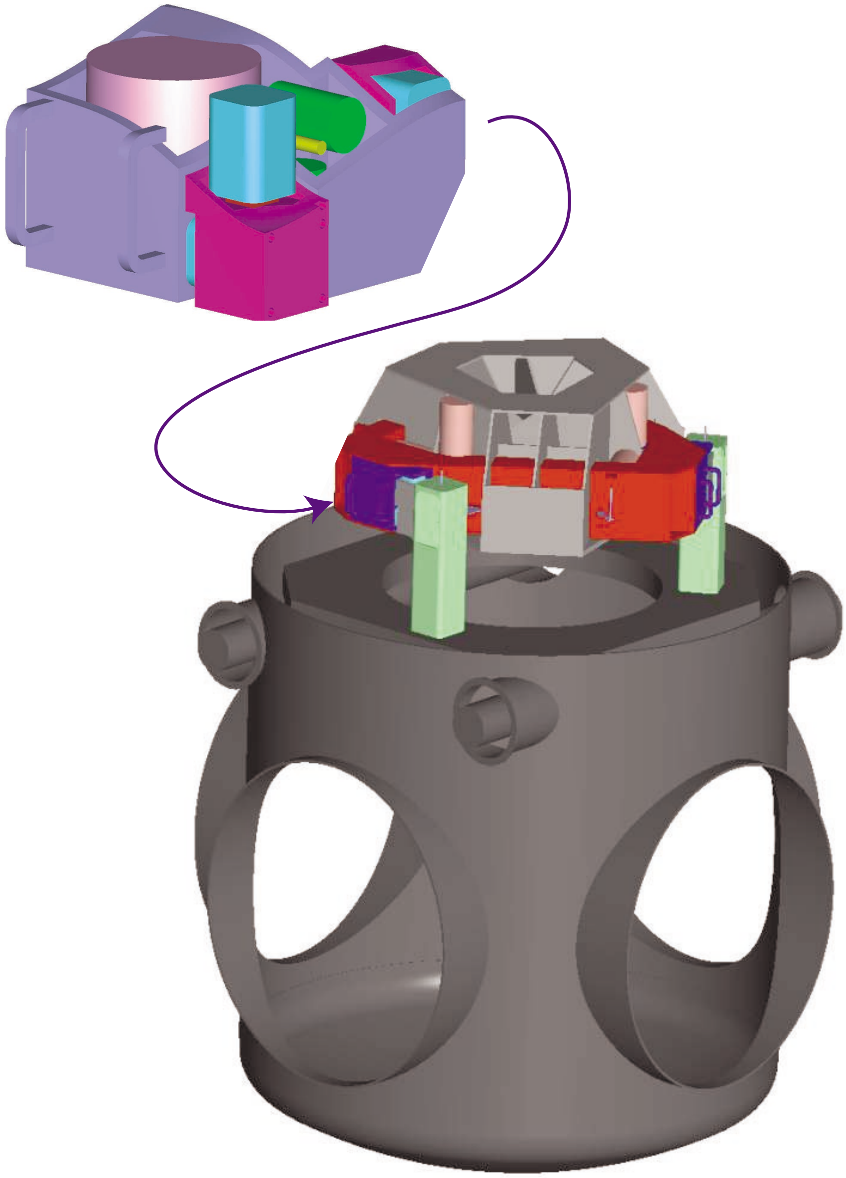

Figure 4: Rendering of BSC design of the two-stage active platform, shown without the surrounding BSC. The blue inner stage is built around the optics table interface that supports the suspension pendulums that hang down through the hole shown in the gray SEI support table. The height shown is correct for the current SUS design. The inset at left shows one of the field-removable instrumentation pods, common to both platform configurations, that houses the STS-2 long-period seismometer (pink), actuator magnet and coil (blue), and small geophones (green). The only instruments outside this pod, the large GS-13 geophones, are mounted directly on the inner stage.

of these sensors will need to be encapsulated in small chambers filled with trace gas, complete with electrical feedthroughs; this is accomplished largely by confining them to the pod drawer. Some parts, such as the "target" side of the capacitive sensor don't require encap-

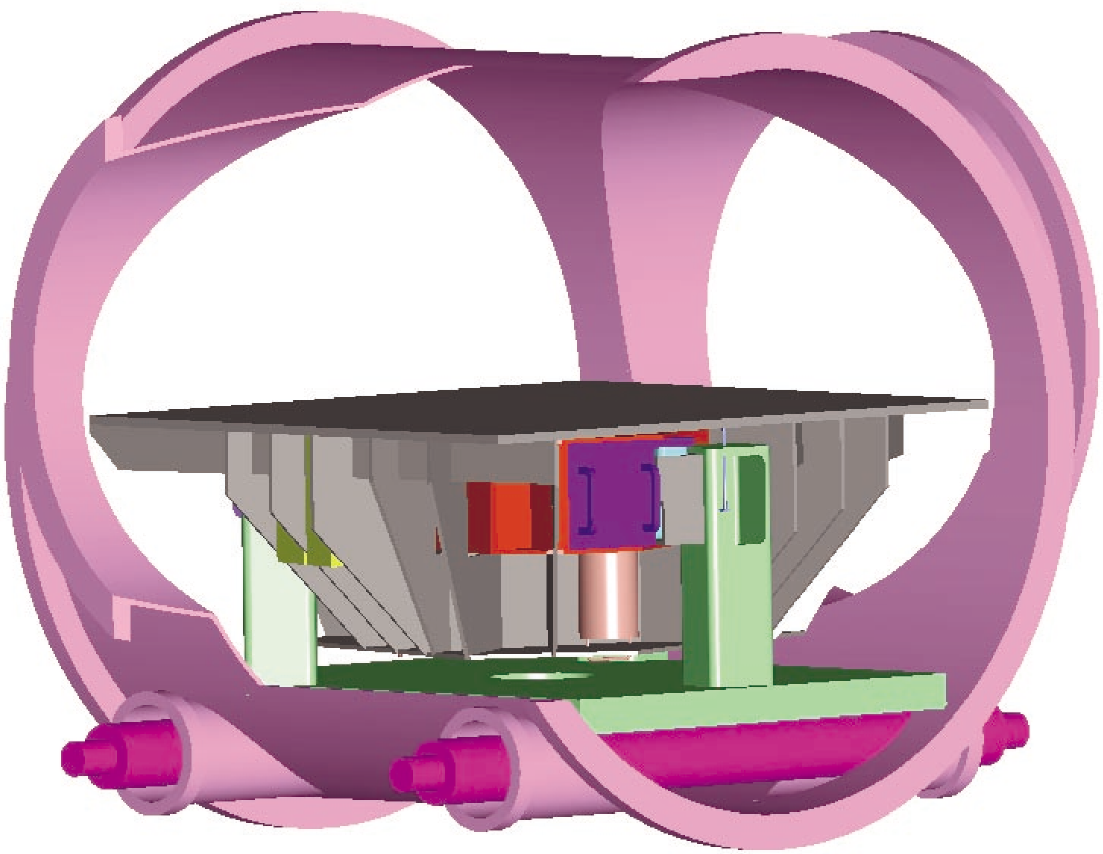

Figure 5: Rendering of the HAM design. Note that the instrumentation pods are positioned so that they are removable through the large HAM doors. The inner stage optics table (blue) is the same size as the table in LIGO-I, and in the same position. (This table height is 8 cm higher than the requirements in this sketch; there is sufficient flexibility to lower it, however.)

sulation. The equivalent displacement noise levels for these sensors are shown in Fig. 6.

Capacitive bridge sensor: To measure the relative displacement between adjacent SEI stages, we intend to use an off-the-shelf sensor such as the Queensgate NXD NanoSensor, which has a 1.25 mm range and a noise level of 1.8×10^{-10} m/$\sqrt{\text{Hz}}$. This Queensgate sensor's form is a thin 2 cm by 2 cm square, and it measures displacement with respect to a similarly sized metal plate using a capacitance bridge. This sensor is available in a vacuum compatible version.

Streckeisen STS-2: Figure 7 shows the STS-2 seismometer manufactured by Streckeisen AG. It is the standard for low-noise, very broadband seismological measurements. The casing is a cylinder 23.5 cm in diameter and 26 cm tall, and it houses three identical proof masses, arranged symmetrically about a vertical axis. Each proof mass is held in the center of its range by a servo using capacitive sensing and coil/magnet actuation; the servo error

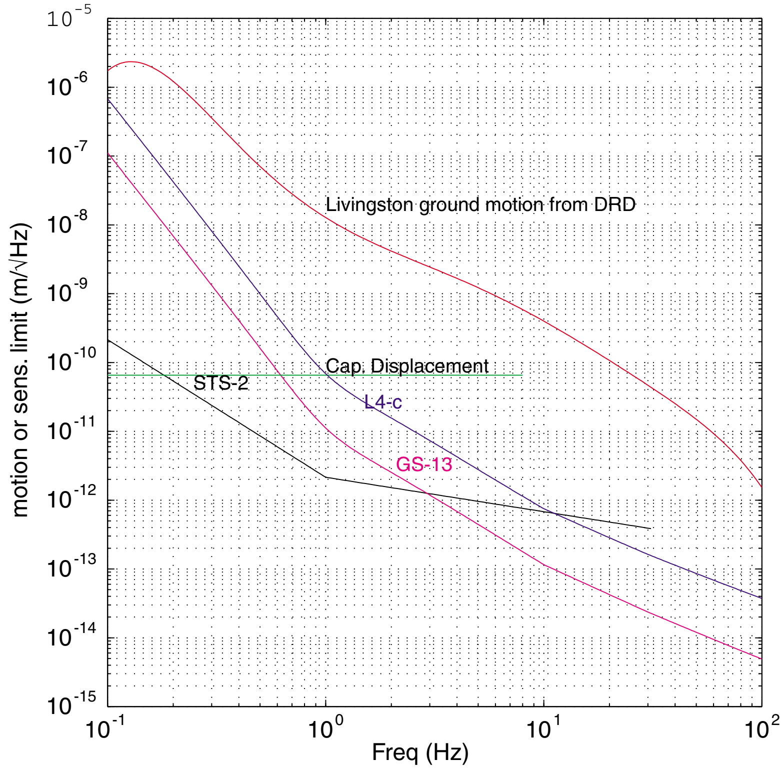

Figure 6: Displacement noise in various sensors used in the two-stage active isolation platform, compared with the DRD spline fit to noise at LLO (which is noisier than LHO at nearly every frequency). Note that the STS-2 can resolve motion approximately 4 orders of magnitude below the ground noise at microseismic frequencies.

signal is a measurement of the ground motion. The signals from the three proof masses are electronically combined to give two orthogonal horizontal outputs and one vertical output. The response of the servo is tailored to give an approximately flat velocity response from 20 mHz to 50 Hz. In this frequency regime, the linear range of the seismometer is enormous, around 26 mm/s. The noise floor can be seen in Figure 6; it is several orders of magnitude below typical seismic noise at 0.1 Hz. There are no internal mechanical resonances below 100 Hz. The STS-2 may be operated in vacuum. However, we anticipate enclosing it in a sealed case for the Advanced LIGO application. We currently have nine of these units, enough to carry us through the R&D phase of advanced LIGO.

Geophone: The GS-13 seismometer manufactured by Geotech Instruments LLC is a low-noise geophone. Its package is identical to that of the widely used (over 5000 units in the field) S-13 seismometer made by the same company: a cylinder 17 cm in diameter and 38 cm from base to handle. It is convertible between horizontal and vertical operation, and has a natural frequency adjustable between 0.75 and 1.1 Hz. The noise floor is shown in Fig. 6. The seismometer is designed to be submersible and may be operated in vacuum, though for use in LIGO we anticipate housing it in a separate sealed enclosure with a preamplifier. Each unit has a mass of 10 kg.

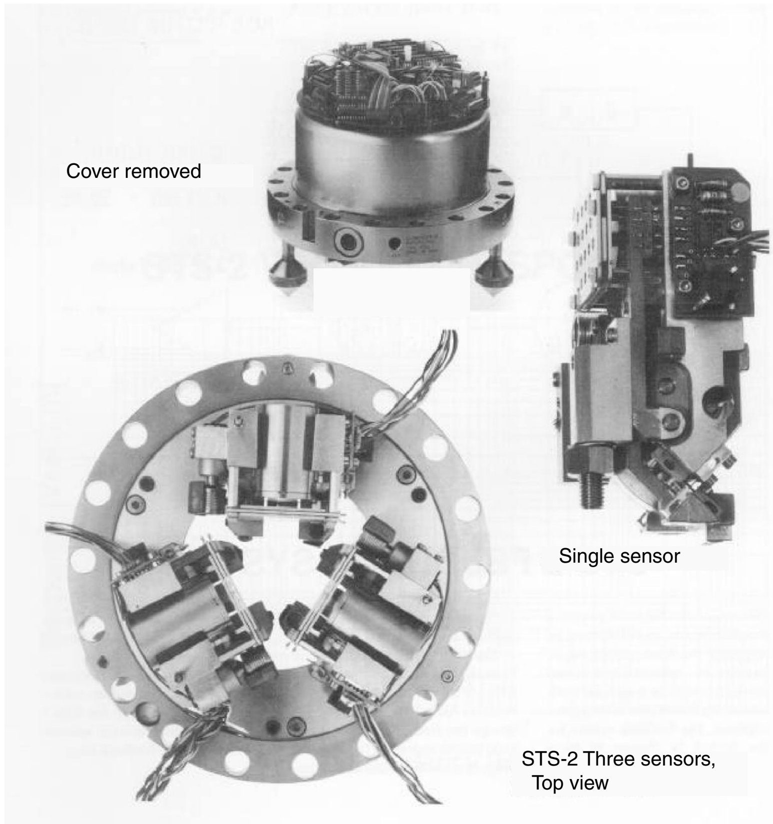

Figure 7: A broadband long-period vibration sensor usable from tens of millihertz to tens of hertz. Each STS-2 seismometer, manufactured by Streckeisen AG, measures vibration in three degrees of freedom. A vacuum-tight domed cover is included but not illustrated here. Sz. Marka is developing a remote mass locking device for the STS-2.

Magnetic actuators: Our pre-prototype experiments have used non-contacting voice coil and permanent magnet forcers, some homemade and some made by BEI Kimco. There are two kinds, a round voicecoil dipping into a radial magnetic field, and a rectangular coil moving in a field that is approximately constant on two opposite sides of the rectangle. Both types are available off-the-shelf, though the round design is offered in a greater variety of sizes and with larger magnet gaps (and therefore actuation range), so was chosen for our pre-prototype tests.

The rectangular design offers reduced magnetic emission, as well as less cross-coupling of force between the stroke and transverse axes. For this reason, we plan to procure custom-made forcers of this type for Advanced LIGO, so we can have the desired large gaps in an interference-resistant configuration. Prototype quantities are being ordered from BEI for use in the ETF prototype.

	displacement	pitch	yaw
ASD at 10 Hz	2×10^{-13} m/$\sqrt{\mathrm{Hz}}$	4×10^{-13} rad/$\sqrt{\mathrm{Hz}}$	4×10^{-13} rad/$\sqrt{\mathrm{Hz}}$
RMS deviation	1×10^{-11} m	3×10^{-11} rad	2×10^{-11} rad
RMS velocity	1×10^{-10} m/s		

Table 1: Key noise levels calculated for the two-stage active isolation platform, without the beneficial effects of the hydraulic stage and feedforward. The RMS noise is calculated by integrating the amplitude spectral density down to 1 Hz; See graphs in other figures for additional values.

3 Performance model

We have used Matlab-based modeling tools [3] to make a preliminary prediction of the performance of the double active stage within the vacuum system. The motions of the stages are modeled in all DOF (a total of $6 \times 2 = 12$). We have fitted the stages with an array of sensors and actuators, and the control is accomplished with twelve single-input single-output (SISO) loops. This model is therefore conservative, not taking into account any benefits that may be obtained with multi-input multi-output techniques and feed-forward.

Although these are preliminary results, they should accurately represent the performance of the two-layer active platform, without feedforward; they are summarized in Table 1.

3.1 Model results summary

Since [1] and [3] were released, the model has been extensively revised, largely because our pre-prototype experiments have challenged it with real data. The most important changes are the inclusion of the tilt sensitivity of horizontal seismometers, and a much more detailed description of the pre-stressed blade springs and their attachment links and flexures. The combination of these two features allows us to study systems that have realistic mechanical cross-coupling between horizontal and tilt motion, as well as cross-coupling in the sensors.

As could be expected, there is potential for instability or near-instability. The latest model for our reference design intentionally includes a 1 mm vertical offset between the blade spring's neutral plane and the upper effective flexure point of the rod that supports its load, as well as a 1 mm vertical offset between the plane of the horizontal actuators and the lower flexure. These tolerances are thought to be easy to achieve without excessive adjustment in the installation process. As is shown in Fig. 8, we have found that our current design is susceptible to a low-Q (half cycle), of order 100 second, ringing in the horizontal direction in response to a tilt step function. The amplitude of this is approximately 500 μm per μradian. Measurements in the VEA at LLO indicate that tilt of order 1 μrad can be induced by moving a 9000 pound fork truck right up to the tank. A person, or even a group of people, would produce less than 1/20 of this. So, the fork truck might be expected to cause a slow 0.5 mm excursion, and the people might cause one of 25 μm. We expect that the latter motion might easily be suppressed in the test mass chambers if ISC global signals are fed back to the SEI stages. Even the fork truck would not cause the active platform to exceed its dynamic range. We expect[12] that the native ground noise tilt, which peaks

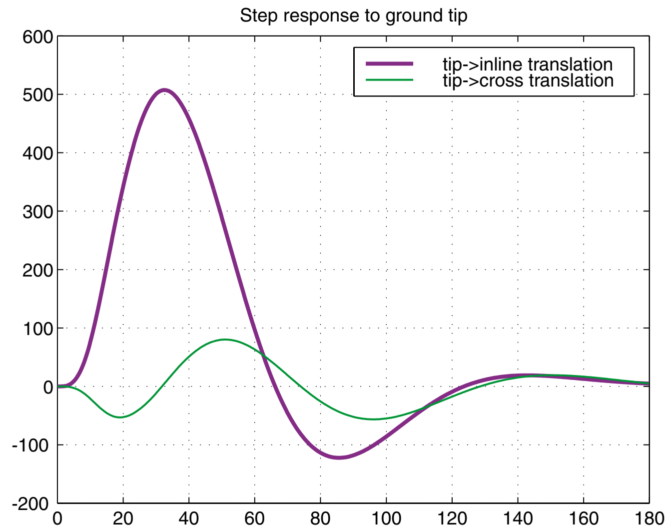

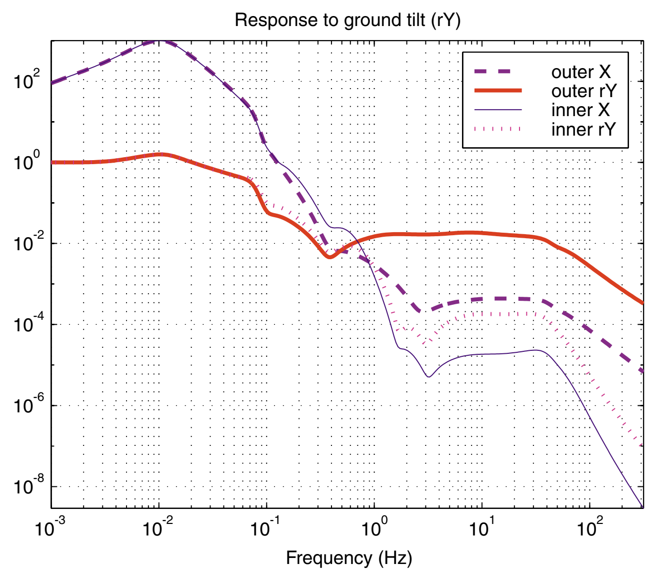

Figure 8: Tilt-horizontal coupling at very low frequencies. Small mechanical cross-coupling combined with tilt pickup in horizontal seismometers can create a fairly large horizontal excursion in response to a tilt step function on the ground. The upper graph shows this in the time domain, and the lower graph shows the transfer function between tilt input and various outputs.

at the microseism, filtered by the technical slabs, will be below 1×10^{-8} rad/$\sqrt{\text{Hz}}$, so the tilt-horizontal ringing should not be a problem in normal operation. (Unfortunately, this slab tilt amplitude seems to below what we can measure with our PEM tilt meters, which are very good at measuring horizontal acceleration at these frequencies.)

This tilt-horizontal overshoot effect can be made worse by changing the control law and sensor blending to enhance the active ground noise reduction in the microseismic band, and it can be made made better by degrading the noise reduction. It is quite likely that during normal operation the overshoot will never be excited, and the two-stage active platform will meet the isolation requirements as is. During periods of LVEA/VEA activity, the SEI

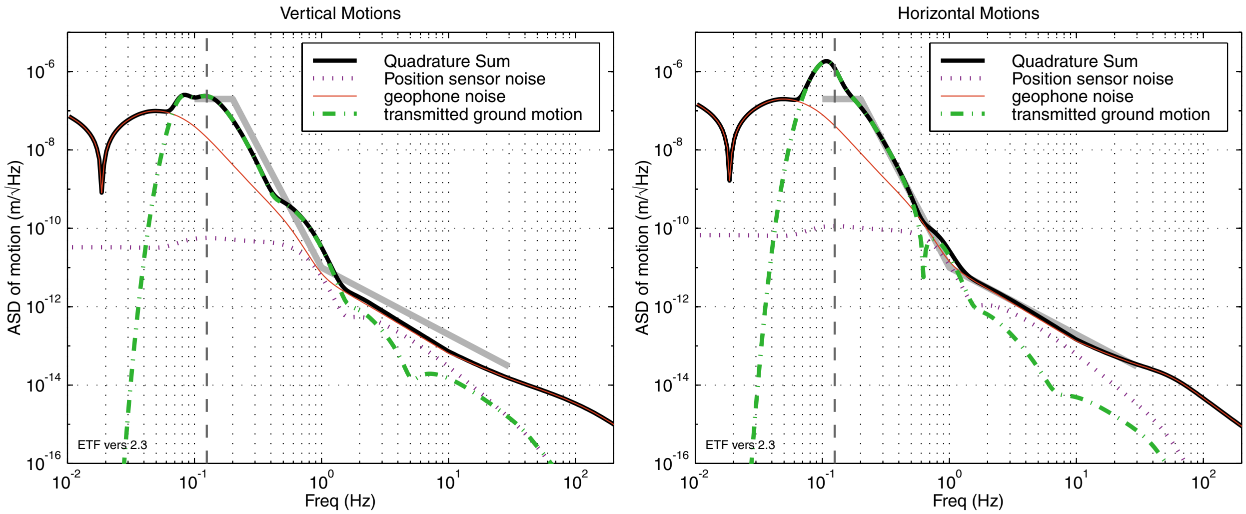

Figure 9: Displacement noise of the two-stage active platform, without feedforward. Here we plot the contributions to the noise level of the SEI optics table, the suspension system mounting point.

systems would likely be placed in a mode optimized to minimize the overshoot.

There are several other techniques that may be explored, in order to increase our tolerance of excess tilt step in the low-noise mode. We can measure the tilt directly, perhaps on the external SEI frame, and use this signal to correct the internal seismometer signals. Alternatively, we can close a low-bandwidth tilt servo loop on the external frame using the hydraulic actuators. Either of these methods would require tilt sensors better than the current PEM sensor. The most promising way to measure the tilt signal is by subtraction of two horizontally-separated STS-2 vertical signals. Alternately, one could use a sensor similar to that described in [13], an instrumented dumbbell suspended near its center of mass. Although designed for slightly higher frequencies, this device is highly insensitive to horizontal acceleration. Similar instruments are under development by VIRGO and GW group in Perth.

3.2 Model details

Arrangement of the sensors: The sensors and actuators are placed on the stages at the actual design positions so that they sense the real dynamics of the platforms at the sensed position, not the idealized translations at the mass center. This means the model can properly simulate the coupling of the various rigid-body modes of the plant into the sensors and actuators.

Relative position sensors: The low frequency sensors we use are relative displacement sensors (e.g., we use the Queensgate NXD NanoSensor in the noise models of the inner active stage). Relative position sensors improve the stability of the system by eliminating low frequency cross-overs in the servo compensation loops. However, since they are relative position sensors, they effectively lock the stages together over the frequency range where they provide the dominant loop gain, short-circuiting the isolation of the system. In order

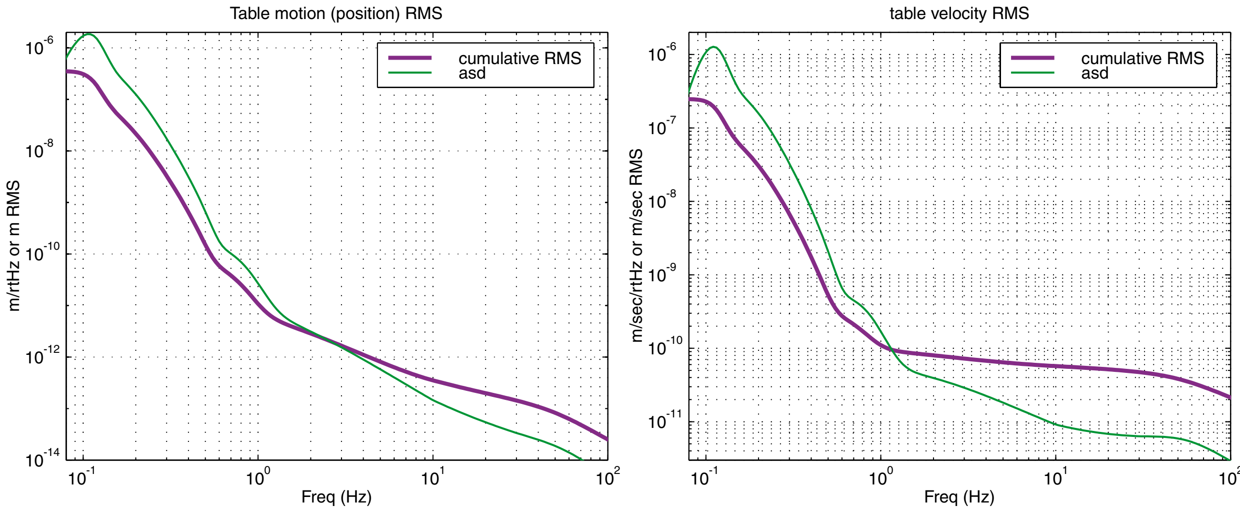

Figure 10: Integral of RMS displacement noise of the SEI optics table.

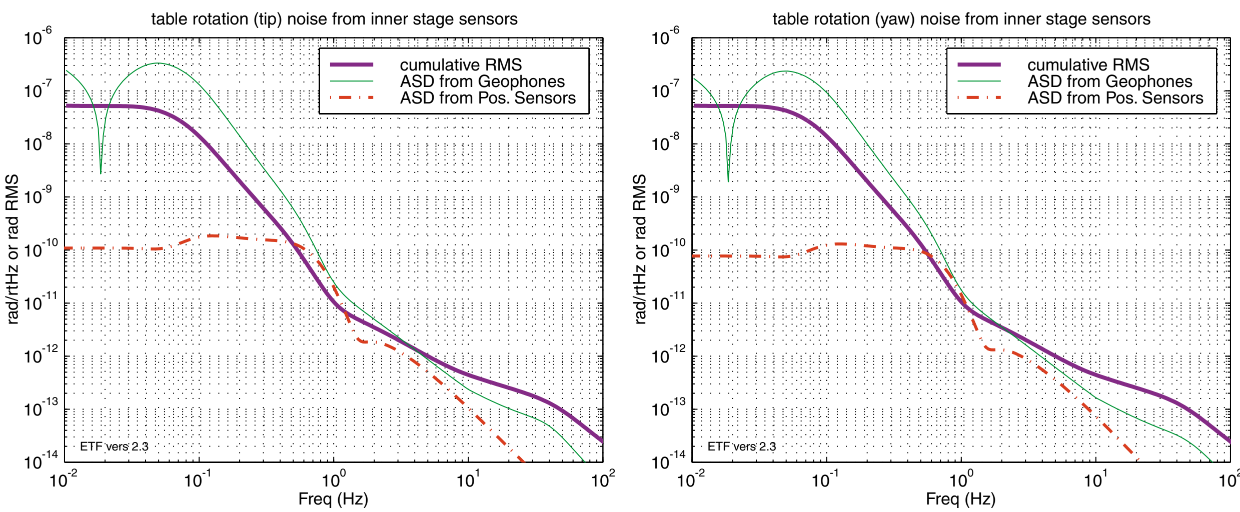

Figure 11: Integral of RMS pitch and yaw motion of the SEI optics table. Note that these curves assume zero ground excitation.

to properly model the performance of such a system, one must distinguish between relative motions of the isolation stages and absolute motion of the stages in inertial space. The model takes the position sensor signals as the distance, along the vector orientation of the sensor, between sensed points on each platform. As a result, the isolation predictions (see, for example, Fig. 9) correctly indicate that there is no isolation at low frequencies, even though there is high loop gain.

Sensor Noise: The noise from the sensors is one of the basic limits on the performance of the active isolation system. We have modeled the sensor noise for the critical components of the model, the sensors on the inner active stage. The noise models of the sensors are shown in Fig. 6.

Relative Actuators: The model includes the back reaction effects of the forcers which act on the inner active stage. These act by pushing against the outer active stage. The back reaction causes coupling between the inner and outer stage loops, so it must be included to properly model the plant dynamics.

3.2.1 Model structure and component examples

The model of the stiff double-active-stage system can be thought of as a series of functional blocks, illustrated by the Simulink diagram we used to run the model. The model includes several parts:

1. a set of test inputs and outputs.
2. a mechanical model of the two stage system.
3. a set of sensors which are distributed on the outer stage.
4. filters which blend the outer stage sensors into six super-sensors.
5. a set of sensors which are distributed on the inner stage
6. filters which blend the inner stage sensors into six super-sensors.
7. a set of actuators between the outer stage and the ground.
8. a set of actuators between the inner stage and the outer stage.
9. a set of 12 SISO control laws which connect the 12 actuators with the 12 super-sensors.

A typical loop is one of the vertical controllers on the inner stage (stage 2 in Fig. 12). There are two sensors to consider for this loop, the Queensgate relative position sensor, and the GS-13 1 Hz geophone, an inertial instrument. The signals from these two sensors are blended together as shown in Fig. 13.

3.3 Operating modes

The SEI active isolation platform has five operating modes: normal operation, normal without global control input, a high-damping mode for protection and safety during periods extremely high motion, a mode for SEI lock acquisition, and a diagnostics/calibration mode.

Normal operation: Global control signals generated by the ISC interferometers are feed back to the various stages in the SUS. As SUS control signals depart from their quiescent values, control authority is reallocated to the SEI, first to the active platform and finally to the fine hydraulic actuators external to the vacuum system. The goal in designing this reallocation it to keep most sensors and actuators at the center of their range as drifts due to thermal effects and Earth tides change lengths and alignments. Also, as in LIGO-I,

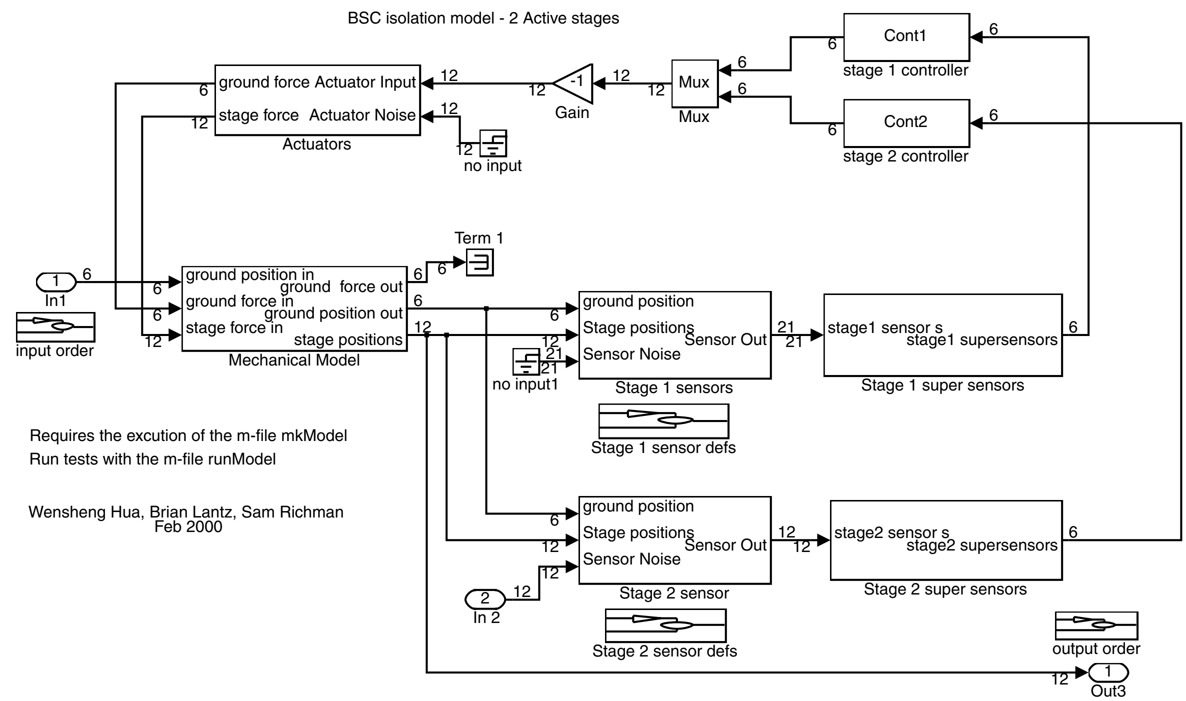

Figure 12: Simulink model used to calculate the dynamics and servo compensation in the conceptual reference design two-stage active platform. Such a design is then used to cross-compile the controller using the dSpace DSP hardware, as is being done in the current pre-prototype experiments. The controllers represented by the blocks Cont1 and Cont2 do not have any coupling between the loops. There is loop interaction because of the nature of the relative position sensors, the actuators, and the mechanical couplings in the double platform. However, by collocating the sensors and actuators, the system is easily controlled with a diagonal compensator (SISO loops).

ground seismometer signals are used to generate a feedforward signal intended to cancel the microseismic motion, and this is applied to the fine actuators. For the "normal operation" mode, the SEI servo compensation is optimized for routine low-noise detector operation.

Normal without global control: During some periods of detector operation is may be necessary to operate the SEI without any global control reallocation, even at extremely low frequencies, and instead take up all of the angle and length drift in the SUS. For this mode, the local position sensors will control the DC position. The capacitive displacement sensors have an RMS position error of order nanometer, so the total position drift in this configuration will likely be limited only by thermal expansion coefficients of the (preexisting) external SEI components and the LVEA/VEA slab. As does the previous mode, this mode still allows low-noise detector operation.

This mode might also be used during ISC lock acquisition.

High-damping, minimum impulse response: During periods of exceptionally large environmental noise, such as during installation when the vacuum system is open, or during

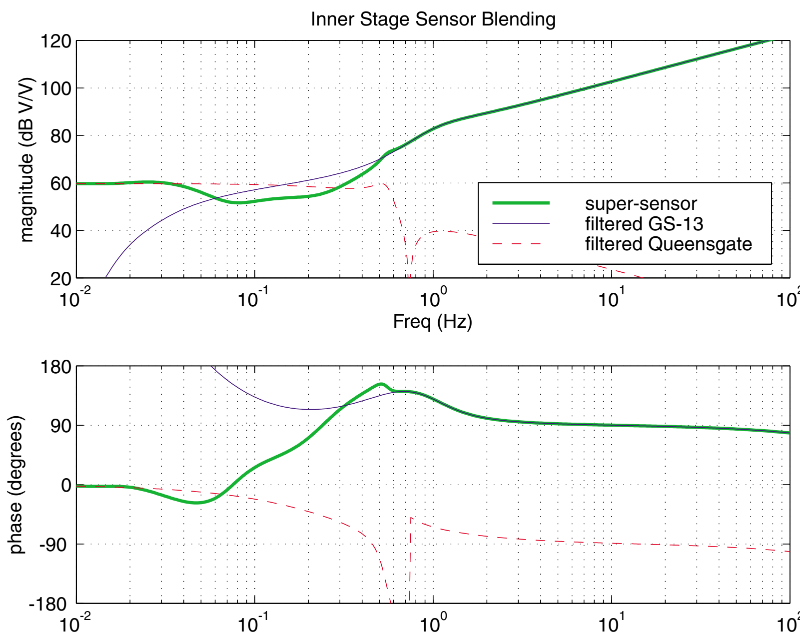

Figure 13: Blending of the inner stage vertical sensors. Aggressive filtering of the sensors occurs once the sensor is no longer the dominant signal source of the loop. This is done to improve the performance of the systems. Additional thought must be given to the blending filters to insure they are robust to reasonable changes in the gain of the sensors. Once the sensors have been combined, they can be thought of as a single, broadband sensor which we call a "super-sensor." The control can then be designed between the 12 actuator inputs to the isolation system, and the 12 super-sensors. The outer stage loops have two blend frequencies (not shown), to combine three sensors into one super-sensor. (This example is not from out latest model.

earthquakes, the system can be switched to a mode where its impulse response is minimized and the servo loops are not destabilized when mechanical range limits are reached. A fail-safe test in the operating code can be programmed to switch the power off if even this mode results in unacceptable motion, thus relying on the hard mechanical limits to limit system damage.

SEI acquire lock This is the mode that systematically closes the active servo loops of the SEI two-stage active platform.

SEI diagnostics and calibration This mode will be used periodically to calibrate the sensors and actuators, and to measure the plant properties; this includes system identification.

4 Other requirements

Vacuum compatibility: The structural elements in the two-stage active platform will be made of the same materials with the same methods as were used to make the LIGO-I SEI

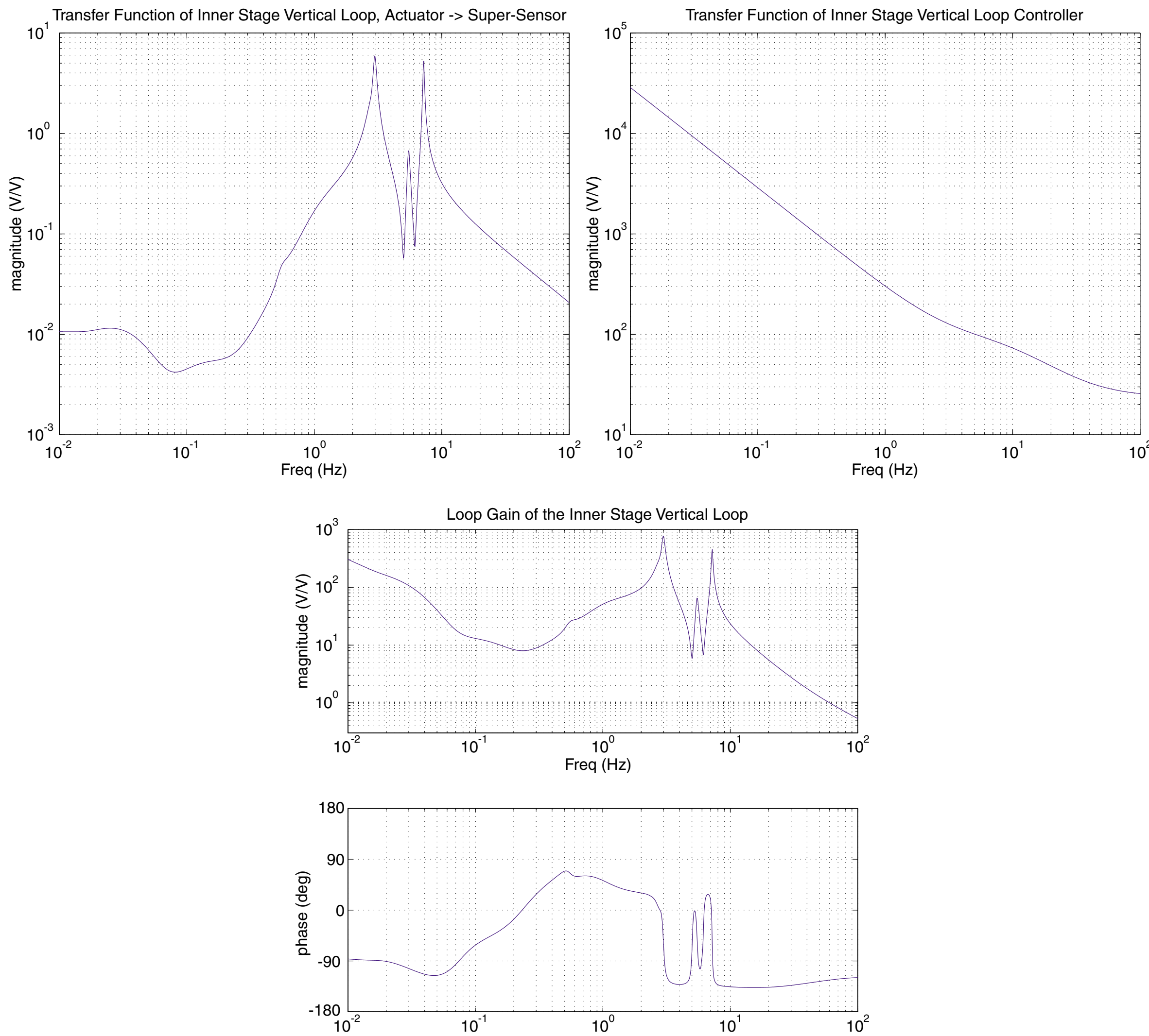

Figure 14: *upper left:* Transfer function from inner stage vertical actuator #1 to its collocated super-sensor. The input and output units are both volts. This system is quite well behaved, so designing a SISO controller is quite simple. *upper right:* A simple system based on an integrator was chosen as the control law. *lower:* This results in a system with an open loop gain which varies between 10 and 30, excluding mechanical resonances. The mechanical resonances are quite large, but are well controlled when all the loops are closed, so the system has only one cross-over, and that upper unity gain frequency is between 60 and 70 Hz, depending on which of the twelve loops you consider.

optics tables and downtube, so we expect there to be no problems with vacuum compatibility in these elements.

The seismometers will be enclosed in sealed chambers within the pods (except for the inner stage GS-13, which has its own enclosure), and filled with trace gas to allow leak testing. The STS-2 dissipates 0.5 W of heat in normal operation; this can easily be removed via copper ribbons, since the dynamics of the "stiff" suspension will be unaffected by reasonable wiring and heat conductors.

The coarse (inductive proximity) position sensors have a working distance of several mm from the metal face, so if necessary the face can be enclosed behind a thin glass window and the rest encapsulated. The fine (capacitive bridge) sensors are available commercially prepared for vacuum use from Queensgate.

The magnet/ voice coil actuators can be prepared for vacuum use, by winding the coils with Kapton-insulated wire.

Cabling accommodation: Wiring for the inside of the vacuum envelope can be exactly as used in LIGO-I. The large number of channels should not be a concern as long as they are routed to prevent rubbing, since the suspension will be much stiffer than the wires. There are obvious surfaces for wire routing (see Figs. 4 and 5).

Earthquake resistance: Figs. 4 and 5 also illustrate the heavy stage frames, which highly constrain the motion of the stages with respect on one another. Heavy stop screws will be adjusted to prevent the voice coils in the actuators from ever touching the magnets. In minor earthquakes, the active isolation system and hydraulic stage are switched to a high-damping mode to limit test mass suspension shaking, even when physical stage-to-stage contact is made.

Diagnostic information: Since every rigid-body degree of freedom is monitored, with a total of 30 measurement channels inside the vacuum system for each SEI, continuous monitoring of diagnostic information comes automatically. These channels can be made available on the reflected memory loop and archived as desired.

Also, as part of the occasional system identification routine necessary for feedforward noise reduction, all transfer functions are measured and can be observed over time for changes and checked against models.

5 Feedback, feed-forward, sensor correction, and all that.

Readers of this document are likely to be familiar with the nomenclature of negative-feedback servo control systems, as they are present in nearly every subsystem of interferometric GW detectors. Since many members of the group producing the design described in this document are from a slightly different school of thought (*i.e.,* Stanford engineering), we have adopted some terms that are new to some in the GW community. These include sensor blending, feed-forward, and sensor correction. There is particular confusion about the last two.

Sensor blending was explained in Section 3.2.1 and is the technique of blending several sensors of the same DOF, each dominating in a different frequency band.

To explain feed-forward and sensor correction, a drawing is helpful. Figure 15 is a generic diagram of a servo control system, and includes the negative feedback path (black), as well as the negative feed-forward path (pink), and a sensor correction block (blue) in the feedback path.

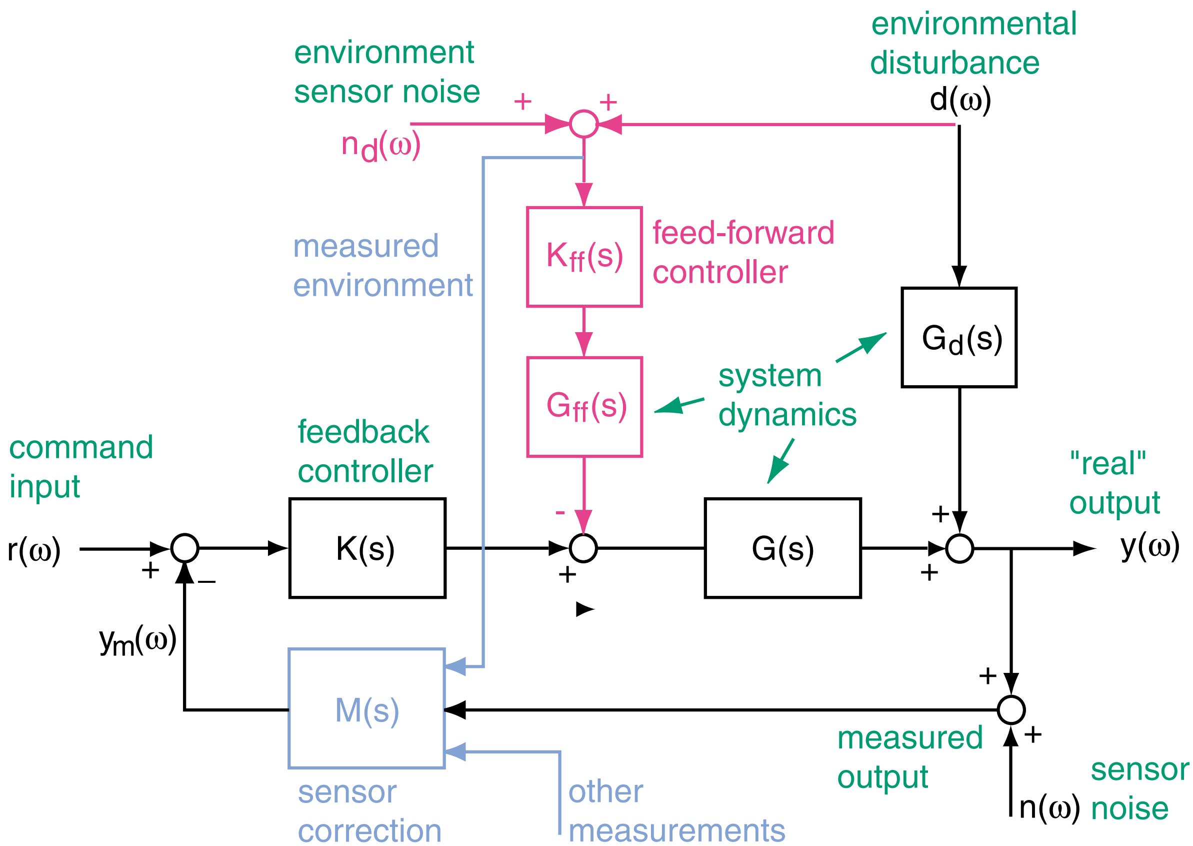

Figure 15: Generic servo control system. See text.

Simple feedback: Environmental noise, which can come in the form of ground noise, acoustic noise, or even temperature, couples into the system's output y through the dynamics in G_d. We wish to control y to follow r, and close a feedback loop. y is measured with a sensor that adds noise n; this measured value is subtracted from the desired value r, multiplied by the control law K, and applied as a force to the system, which responds with dynamic function G to give its output. With only feedback, the output can be described by the equation,

$$
\begin{aligned}
y \;=\;& (I+GK)^{-1}GK\,r && \text{command tracking}\\
&+(I+GK)^{-1}G_d\,d && \text{disturbance suppression}\\
&-(I+GK)^{-1}GK\,n. && \text{noise}
\end{aligned}
$$

The addition of feedback gain in K suppresses the environmental noise d from the output. If K is sufficiently high, the system tracks r down to a noise floor set by n.

Feed-forward: If $K_{ff}G_{ff}G = G_d$, then the environmental disturbance is removed from the system. While it is true that feedback gain reduces the value at y resulting from the feed-forward correction path by $(I+GK)^{-1}$, the environmental disturbance coupling through

K_d is reduced by the same factor, making feed-forward effective regardless of the feedback scheme.

Sensor correction: When a particular sensor's output is corrupted by either environmental noise or unwanted DOF's, the block M can be used to subtract off these things, leaving a "best guess" measurement for use in the feedback path. Two examples of this corruption can be seen in our system, ground motion coupling into the relative position sensors by shaking the SEI frame, and the pitch or yaw DOF's being sensed at low frequencies as horizontal motion in the seismometers. Each of these can at least partially be corrected. In the case of position sensor correction, we can measure the motion of the frame with a seismometer to provide the correction signal. In the case of the tilt-sensitive seismometers, we can either use a tilt sensor or subtract horizontally-spaced sets of vertical seismometer signals (which makes the system MIMO).

Sensor correction differs fundamentally from feed-forward in that it does nothing to the system unless the feedback loop is active. Badly implemented sensor correction can also destabilize the feedback control; feed-forward, done badly, just adds noise.

6 Pre-prototype results

6.1 Hydraulic actuators

Two full-sized actuators have been built and tested at Stanford. The actuators are mounted in a test stand (Fig. 16) and are used to move a 360 kg test load that is suspended with stiff springs from the stand. This apparatus has demonstrated appropriate noise levels, force levels, and servo bandwidth.

6.2 Active isolation platforms

Two pre-prototype experiments are currently running to develop technology and test concepts for the in-vacuum active isolation platform. The first, currently operating next to the Stanford ETF and shown in Figure 17, is a single active isolation stage supporting two back-to-back GEO600-size pendulum suspensions. The active isolation platform features highly collocated geophone sensors, relative position sensors and magnet-voicecoil actuators, and principally uses six SISO loops to quiet itself. The goals of this experiment include the detailed exploration of sensor blending, feed-forward and sensor correction techniques, as well as validation of the model used in the Hua/Lantz Matlab simulation code. Also, this apparatus has been used to demonstrate joint operation of triple pendulum damping loops and active seismic isolation of the pendulum mounting platform.

It has been in operation for over a year, and has largely met its goals. In particular, it was shown that the small perturbations that the SEI and SUS loops make on each other's plant didn't prevent each from operating independently of the other, at least for this pre-prototype's particular configuration. (In the case of Advanced LIGO, we expect that same will be true, though this cannot be explored until each design matures a bit.) The investigation of position sensor correction with measured ground motion has also yielded promising

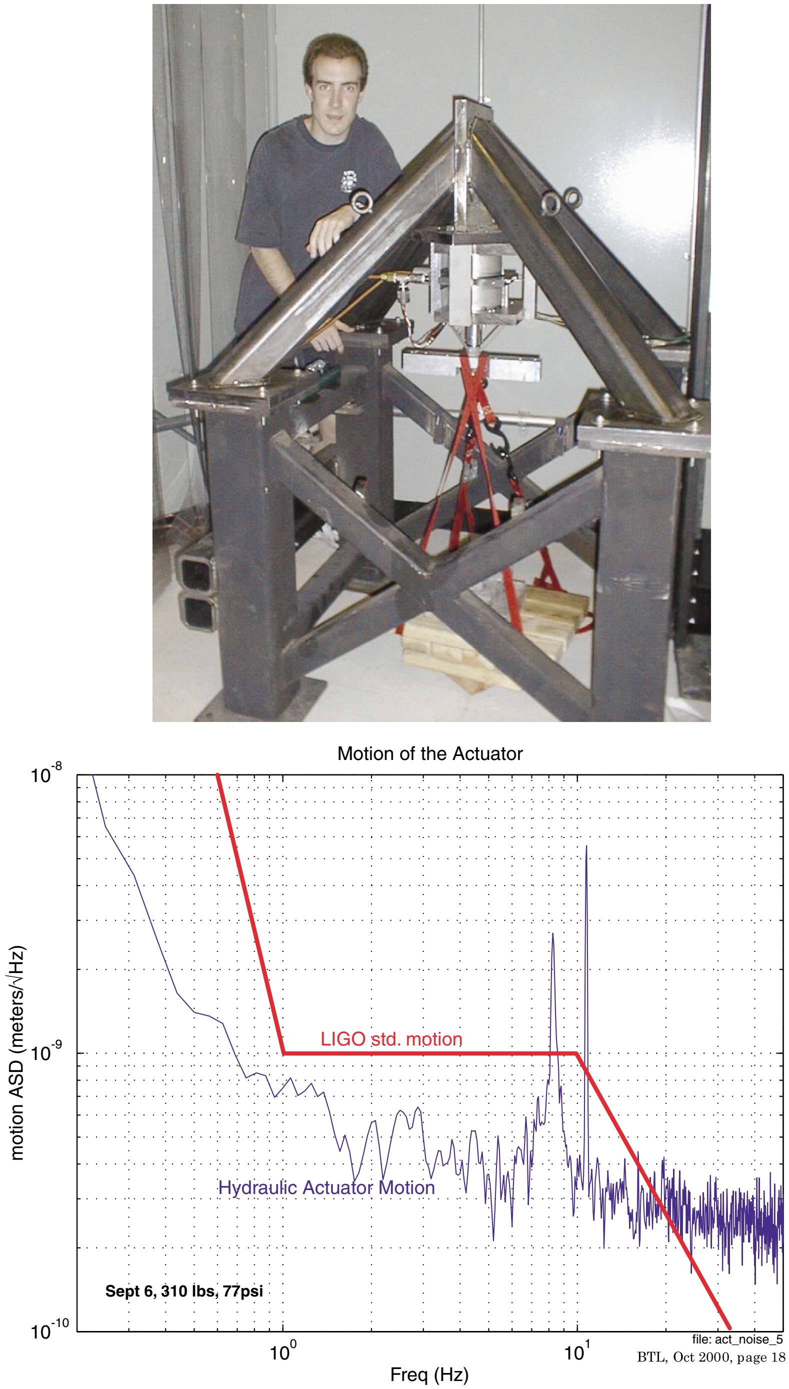

Figure 16: Test frame for hydraulic actuators, before large load was installed, along with a plot of the maximum-force, open-loop response of a hydraulic actuator attached to its design load. Low-frequency noise will be suppressed by using local feedback to a position sensor.

results. The graph in Fig. 17 shows the uncontrolled vertical transmission of ground displacement noise (blue), the transmission with conventional SISO feedback (pink), and the transmission with both feedback and sensor correction (green), together with the model's

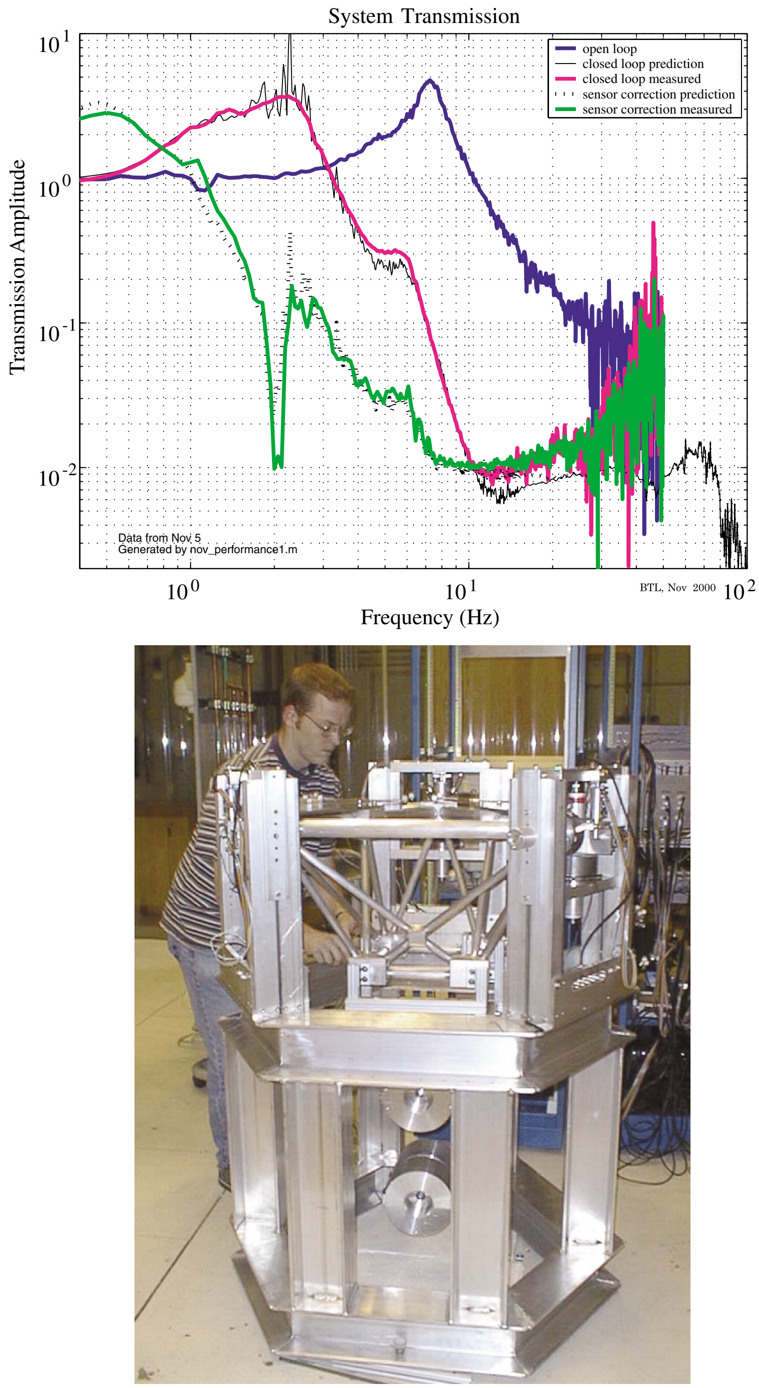

Figure 17: The Stanford single-stage active isolation platform supporting a dual triple pendulum of the GEO600 design. Plotted are the effects of active isolation and sensor correction using a floor-mounted seismometer. See text.

predictions (dashed lines).

Another experiment is underway next to the LASTI system at MIT (Figure 18), in a large vacuum tank. It is intended to demonstrate two crucial aspects of our conceptual design that had not been present in the apparatus from [7], and to serve as another case for model validation. Although the JILA experiment used 12 SISO active isolation loops, it

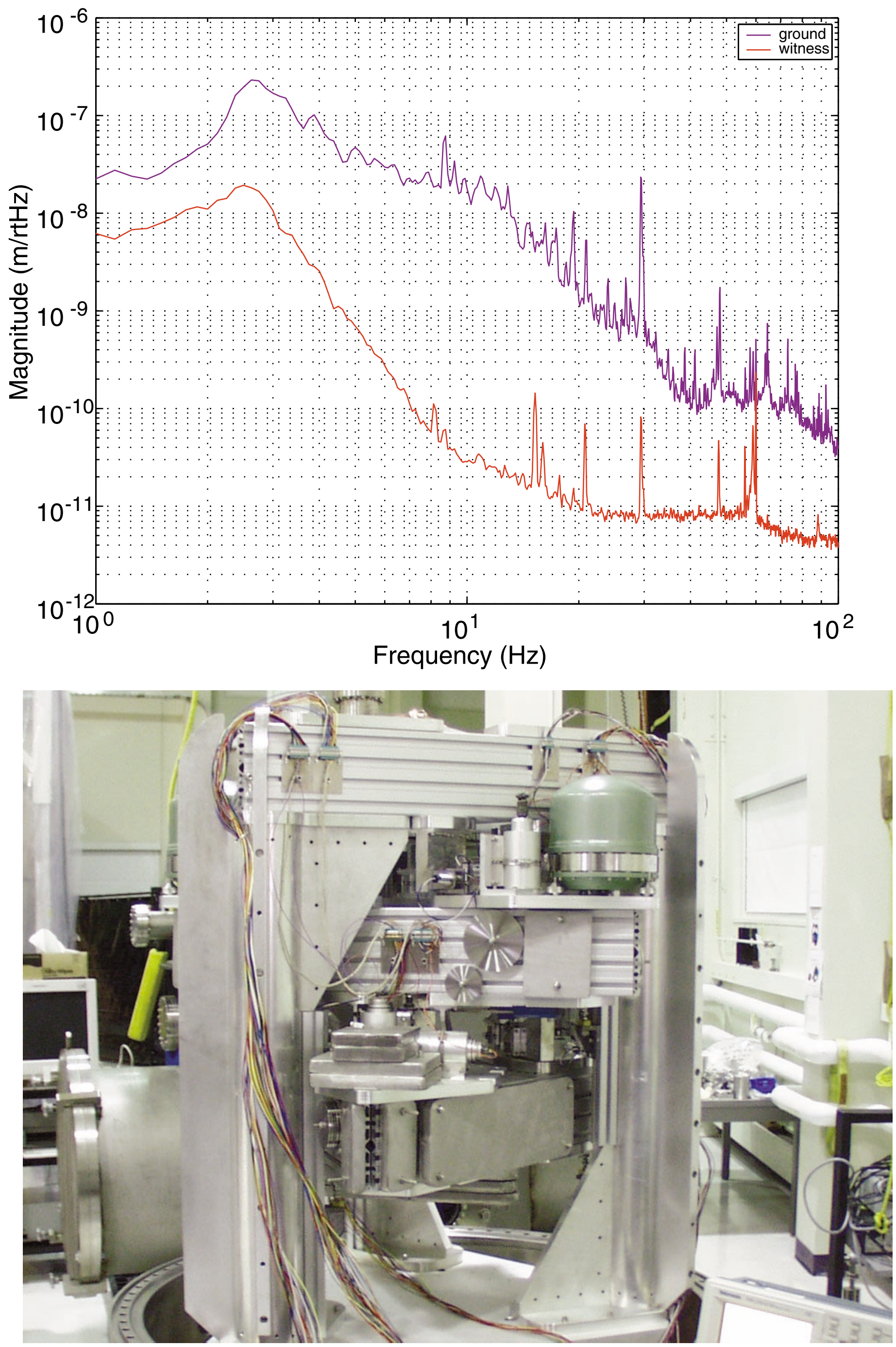

Figure 18: The two-stage active isolation experiment under operation at MIT. The two stages can be seen in the photograph, the upper one featuring the green domed STS-2 on the near corner. Vertical ground noise (purple) and payload noise (red) are plotted above.

was a proof-of-principle experiment and was not optimized for extended operation. The two-stage experiment in operation at MIT was specifically designed with the dynamic range and low thermal sensitivity necessary to stay in lock for long periods, and it has been operated for tens of hours at a time in the presence of extremely large floor motion adjacent to a construction site.

The other performance goal of this experiment is to show about an order of magnitude reduction of the microseismic peak. This has been demonstrated in preliminary data, but work remains before it can be quantitatively described. Figure 18 contains a graph of this system's displacement noise (red) together with the floor motion below, in the vertical direction. The horizontal performance is similar.

7 Conclusions and development strategy

7.1 Performance

Generally the modelling of the in-vacuum two-stage active isolation platform indicates that without any additional noise control from an external hydraulic stage most of the requirements set out in [2] can be met or nearly met.

Isolation performance: The unlabeled grey lines drawn in Figure 9 in this report correspond with the requirements from Figure 2 in the current DRD [2]. Where the currently modelled system exceeds the requirements, it is due to insufficient ground noise suppression (i.e., loop gain), not due to having reached the noise floor of our sensors. In high ground noise locations, like the LASTI lab at MIT, additional isolation could be helpful, depending on the experimental goals.

RMS motion requirements: The RMS displacement level integrated down to 1 Hz shown in Fig. 10 are approximately 1×10^{-11} m; This appears to be sufficiently small to allow low-bandwidth LSC loops in Advanced LIGO.

The RMS angular noise from the SEI sensor noises and ground integrated down to 1 Hz is shown in in Fig. 11. Note that these curves assume zero ground excitation, since we don't really know how large the angular motion is on our technical slabs. It will probably be $< 1 \times 10^{-8}\mathrm{rad}/\sqrt{\mathrm{Hz}}$ at the microseism; above that, it is likely to be local human-generated noise. The levels shown in Fig. 11 are well below the needs of the ASC loops, though clearly further study of the local slab angle noise would be interesting (though probably not using the PEM tilt meters).

Actuation requirements: The coarse actuation requirements could clearly be met with the hydraulic external stage. The LIGO-I CAS could also be left in place and used instead. The best way to carry out fine actuation to offset the Earth's tides and extraordinary microseismic motion or "nuisance" earthquakes is probably the hydraulic system. However, the LIGO-I piezoelectric FAS, once it proves to be effective, can also be considered for this role.

Transient performance: As described in section 3.1, the horizontal seismometers sensitivity to tilt motion can lead to undesirable displacement in response to slow tilt motion.

It is possible that after considering this in view of our planned ISC scheme, we may might want to control tilt more aggressively using the external stage.

7.2 Development needs

As the preliminary and final designs for Advanced LIGO SEI are developed and tested during the next several years (see Figures 19 and 20), we may need to refine our performance requirements based on LIGO-I operational experience with transient noise and how it affects duty cycle. This may help us to decide how many (if any) tanks are fitted with external hydraulic stages.

Preliminary Draft, Advanced LIGO SEI

ID	Task Name	Duration	Start	Finish	Predecessors
1	**Seismic Isolation**	**1504 days**	**Mon 4/3/00**	**Thu 1/5/06**	
2	**SEI Design**	**871 days**	**Mon 4/3/00**	**Mon 8/4/03**	
3	**SEI Conceptual Design/Requirements**	**520 days**	**Mon 4/3/00**	**Fri 3/29/02**	
4	Requirements Definition	44 days	Tue 8/1/00	Fri 9/29/00	
5	**SEI Prototype**	**520 days**	**Mon 4/3/00**	**Fri 3/29/02**	
6	Prototype Design	195 days	Mon 4/3/00	Fri 12/29/00	
7	Prototype Procurement /Fabricatio	128 days	Tue 10/3/00	Thu 3/29/01	11
8	Prototype Modelling	330 days	Mon 4/3/00	Fri 7/6/01	
9	Prototype Assembly / Test	68 days	Fri 3/30/01	Tue 7/3/01	6,7
10	operations development	187 days	Thu 7/12/01	Fri 3/29/02	9,8
11	Conceptual design review	1 day	Mon 10/2/00	Mon 10/2/00	4
12	**Technology Development**	**166 days**	**Fri 8/4/00**	**Fri 3/23/01**	
13	UHV tech development	166 days	Fri 8/4/00	Fri 3/23/01	
14	DSP tech development	57 days	Thu 1/4/01	Fri 3/23/01	
15	Fabrication / materials tech develo	57 days	Thu 1/4/01	Fri 3/23/01	
16	**SEI Preliminary Design**	**632 days**	**Fri 9/1/00**	**Mon 2/3/03**	
17	Sensor Design	66 days	Fri 9/1/00	Fri 12/1/00	
18	Actuator Design	66 days	Mon 10/30/00	Mon 1/29/01	
19	Electronics Design	42 days	Thu 1/4/01	Fri 3/2/01	
20	**SEI/HAM Prelim Design**	**415 days**	**Wed 1/3/01**	**Tue 8/6/02**	
21	System Design/ Simulation	128 days	Wed 1/3/01	Fri 6/29/01	
22	Controls/Software Design	128 days	Wed 1/3/01	Fri 6/29/01	
23	Mechanical Design	83 days	Thu 1/4/01	Mon 4/30/01	
24	Assembly Procedure & Tooling De	140 days	Thu 3/1/01	Wed 9/12/01	
25	Installation Procedure & Tooling D	140 days	Thu 3/1/01	Wed 9/12/01	
26	Preliminary HAM Design Review	1 day	Thu 9/13/01	Thu 9/13/01	9,21,22,23,24,25,1
27	**HAM Pathfinder Fabrication**	**265 days**	**Tue 5/1/01**	**Mon 5/6/02**	
28	fab/procurement plan review	1 day	Tue 5/1/01	Tue 5/1/01	
29	Component fab/procurement	179 days	Wed 5/2/01	Mon 1/7/02	23,13,15,28,14
30	mechanical assembly	62 days	Tue 1/8/02	Wed 4/3/02	29
31	Installation complete	1 day	Thu 4/4/02	Thu 4/4/02	30
32	controls checkout	22 days	Fri 4/5/02	Mon 5/6/02	10,31
33	HAM Pathfinder Testing	66 days	Tue 5/7/02	Tue 8/6/02	32
34	**SEI/BSC Prelim Design**	**415 days**	**Tue 7/3/01**	**Mon 2/3/03**	
35	System Design/Simulation	129 days	Tue 7/3/01	Fri 12/28/01	
36	Controls/Software Design	129 days	Tue 7/3/01	Fri 12/28/01	
37	Mechanical Design	85 days	Wed 7/4/01	Tue 10/30/01	
38	Assembly Procedure & Tooling De	137 days	Mon 9/3/01	Tue 3/12/02	
39	Installation Procedure & Tooling D	137 days	Mon 9/3/01	Tue 3/12/02	

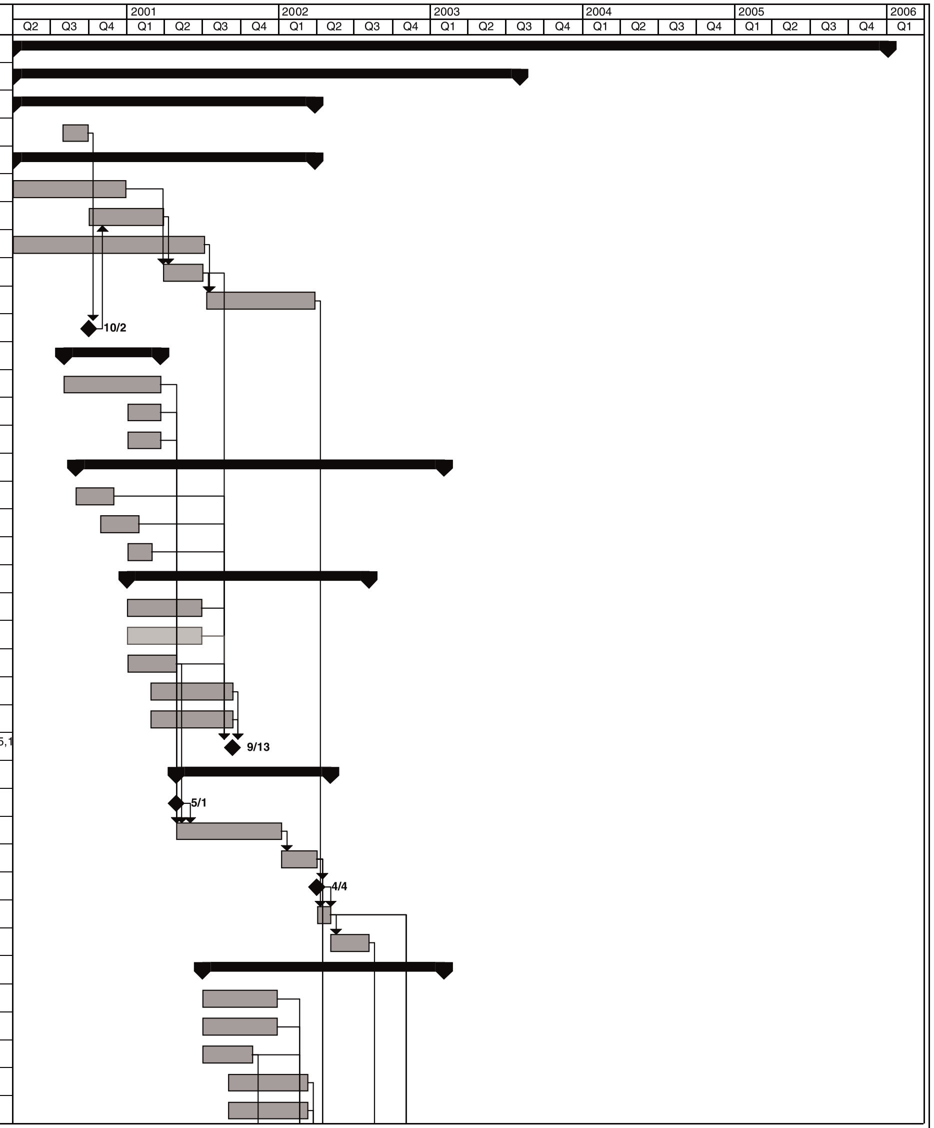

Project: SEI_project
Date: Fri 8/25/00

Task | Split | Progress | Milestone | Summary | Rolled Up Task | Rolled Up Split | Rolled Up Milestone | Rolled Up Progress | External Tasks | Project Summary

Page 1

Figure 19: SEI R&D Schedule, page 1

Preliminary Draft, Advanced LIGO SEI

ID		Task Name	Duration	Start	Finish	Predecessors
40		Preliminary BSC design review	1 day	Wed 3/13/02	Wed 3/13/02	39,35,36,37,38
41		**BSC Pathfinder Fabrication**	**263 days**	**Thu 11/1/01**	**Mon 11/4/02**	
42		fab/procurement plan review	1 day	Thu 11/1/01	Thu 11/1/01	
43		Component fab/procurement	176 days	Fri 11/2/01	Fri 7/5/02	37,42
44		mechanical assembly	63 days	Mon 7/8/02	Wed 10/2/02	43
45		Installation complete	1 day	Thu 10/3/02	Thu 10/3/02	44
46		controls checkout	22 days	Fri 10/4/02	Mon 11/4/02	45
47		BSC Pathfinder Testing	65 days	Tue 11/5/02	Mon 2/3/03	46
48		**SEI Final Design**	**347 days**	**Wed 4/3/02**	**Sat 8/2/03**	
49		Sensor Design	130 days	Tue 11/5/02	Mon 5/5/03	46,32
50		Actuator Design	130 days	Tue 11/5/02	Mon 5/5/03	46,32
51		Electronics Design	130 days	Tue 11/5/02	Mon 5/5/03	46,32
52		**SEI/HAM Design**	**217 days**	**Wed 4/3/02**	**Sun 2/2/03**	
53		System Design/Simulation	180 edays	Tue 8/6/02	Sun 2/2/03	33
54		Mechanical Design	180 edays	Wed 4/3/02	Mon 9/30/02	30
55		Assembly Procedure & Tooling De	180 edays	Wed 4/3/02	Mon 9/30/02	30
56		Installation Procedure & Tooling D	180 edays	Wed 4/3/02	Mon 9/30/02	30
57		**SEI/BSC Design**	**217 days**	**Wed 10/2/02**	**Sat 8/2/03**	
58		System Design/Simulation	180 edays	Mon 2/3/03	Sat 8/2/03	47
59		Mechanical Design	180 edays	Wed 10/2/02	Mon 3/31/03	44
60		Assembly Procedure & Tooling De	180 edays	Wed 10/2/02	Mon 3/31/03	44
61		Installation Procedure & Tooling D	180 edays	Wed 10/2/02	Mon 3/31/03	44
62		SEI Final Design Review	1 day	Mon 8/4/03	Mon 8/4/03	48,52,57
63		**SEI Fabrication**	**614 days**	**Mon 9/1/03**	**Thu 1/5/06**	**62**
64		Mechanical Fabrication	261 days	Mon 9/1/03	Mon 8/30/04	
65		Electronics Fabrication	261 days	Mon 9/1/03	Mon 8/30/04	
66		Software Coding	261 days	Mon 9/1/03	Mon 8/30/04	
67		First Article Testing	91 days	Tue 8/31/04	Tue 1/4/05	64,65,66
68		Assembly	262 days	Wed 1/5/05	Thu 1/5/06	67

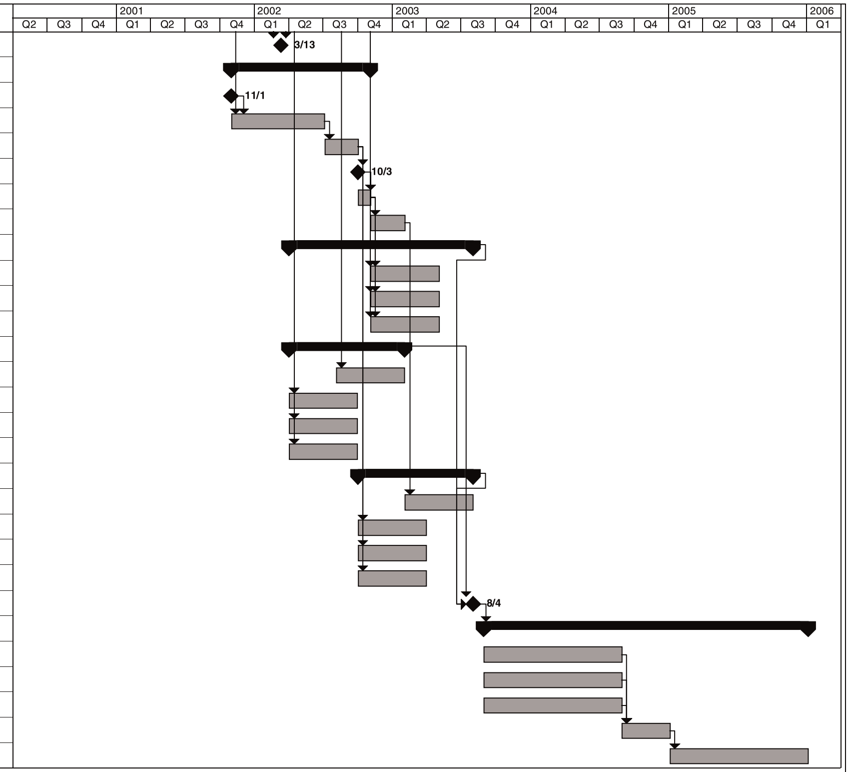

Project: SEI_project
Date: Fri 8/25/00

Task | Progress | Summary | Rolled Up Split | Rolled Up Progress | Project Summary
Split | Milestone | Rolled Up Task | Rolled Up Milestone | External Tasks

Page 2

Figure 20: SEI R&D Schedule, page 2

References

[1] J. Giaime, B. Lantz, S. Richman, D. Debra, C. Hardham, J. How, and W. Hua, "Baseline LIGO-II implementation design description of the stiff active seismic isolation system." 3/8/2000. LIGO-T000024-00-U

[2] D. Shoemaker, D. Coyne, "LIGO-II Seismic Isolation Design Requirements Document." 11/4/1999. LIGO E990303-02-D,

current version: P. Fritschel, D. Coyne, J. Giaime, B. Lantz, D. Shoemaker, "Seismic Isolation Subsystem Design Requirements Document." 1/17/2001 LIGO-E990303-03-D

[3] Brian Lantz, Wensheng Hua, Sam Richman, Jonathan How, "Computer Modeling and Simulation in Support of the Stiff-Suspension Active Seismic Isolation for LIGO II," 2/14/2000, LIGO T000016-01

[4] Wensheng Hua, Brian Lantz, Sam Richman, "How to construct mechanical model of a mass-spring system," `http://lsuligo.phys.lsu.edu/active/pen3.pdf`

[5] B. Lantz, R. Stebbins, C. Hardham, J. Giaime, "The experimental program in support of stiff-suspension active seismic isolation for LIGO-II," 2/14/2000, LIGO T000015-00.

[6] "LIGO II Suspension: Reference Designs," by the GEO Suspension Team, (distributed within the LSC) 1/31/2000.

[7] Richman, S.J.; Giaime, J.A.; Newell, D.B.; Stebbins, R.T.; Bender, P.L.; Faller, J.E.; "Multi-stage active vibration isolation system," Review of Scientific Instruments, **69:6**, 2531. (June '98)

[8] Hong Sang Bae, "Active Vibration Isolation and Alignment Issues for LIGO," Masters Thesis, Department of Mechanical Engineering, Stanford University, August 1999.

[9] distributed by the GEO suspensions team in January, currently available at `http://www.ligo.caltech.edu/~dhs/l2_sus_ref1.tar`

[10] Peirce, S. Tran, H., Wiedemann, M., and DeBra, D., "Quiet Hydraulics for Ultraprecision Actuation," in Proceedings of ASPE Spring Topical Meeting on Mechanisms and Controls for Ultraprecision Motion, Tucson Az., 1994.

[11] Joshi, S. M., "Robustness Properties of Collocated Controllers for Flexible Spacecraft," AIAA Journal of guidance control and dynamics, **9,** number 1, 85–91. (1986)

[12] Gonzalez, G., "ASC: Environmental Input to Alignment Noise," LIGO-T960103-00-D (July '96).

[13] Speake, C. C., and Newell, D. B., "The design and application of a novel high-frequency tiltmeter." Review of Scientific Instruments, **61:5**, 1500. (May 1990).